

# Finite Membrane Thickness Influences Hydrodynamics on the Nanoscale

Zachary G. Lipel\*

*Department of Chemical and Biomolecular Engineering,  
University of California, Berkeley, California 94720, USA*

*Department of Chemical and Biological Engineering, Princeton University, Princeton, NJ 08544*

Yannick A. D. Omar†

*Department of Chemical and Biomolecular Engineering,  
University of California, Berkeley, California 94720, USA*

*Department of Chemical Engineering, Massachusetts Institute of Technology, Massachusetts 02139, USA*

Dimitrios Fraggedakis‡

*Department of Chemical and Biological Engineering, Princeton University, Princeton, NJ 08544*

(Dated: 05/14/2025)

Many lipid membrane-mediated transport processes—such as mechanically-gated channel activation and solute transport—involve structural and dynamical features on membrane thickness length scales. Most existing membrane models, however, tend to adopt (quasi-)two-dimensional descriptions that neglect thickness-dependent phenomena relevant to internal membrane mechanics, and thus do not fully account for the complex coupling of lipid membranes with their surrounding fluid media. Therefore, explicitly incorporating membrane thickness effects in lipid membrane models will enable a more accurate description of the influence of membrane/fluid coupling on transport phenomena in the vicinity of the bilayer surfaces. Here, we present a continuum model for membrane fluctuations that accounts for finite membrane thickness and resolves hydrodynamic interactions between the bilayer and its surrounding fluid. By applying linear response analysis, we observe that membrane thickness-mediated effects, such as bending-induced lipid reorientations, can generate shear flows close to the membrane surface that slow down the relaxation of nanometer scale shape fluctuations. Additionally, we reveal the emergence of pressure inversion and flow reversal near the membrane interfaces, accompanied by localized stagnation points. Among these, extensional stagnation points give rise to a novel mode of bulk dissipation, originating from bending-induced compression and expansion of the membrane surfaces and their coupling to shear stresses in the fluid. Our findings identify membrane thickness as a key factor in nanoscale hydrodynamics and suggest that its effects may be detectable in fluctuation spectra and can be relevant to interfacial processes such as solute permeability and contact with solid boundaries or other membranes.

*Introduction*—Lipid bilayers form the boundaries of cells and organelles, playing an important role in processes such as endocytosis, cellular adhesion, and action potential propagation [1–5]. Bilayers are commonly modeled as two-dimensional surfaces [6–9], a description that has enabled the study of processes across a wide range of length scales—from membrane budding during endocytosis [10–13] to the diffusion of individual proteins embedded in membranes [14–16]. However, two-dimensional models cannot resolve the internal mechanics and hydrodynamic coupling that emerge at nanoscales, where the membrane thickness becomes the primary intrinsic length scale. For example, thickness deformations are known to mediate protein function through hydrophobic mismatch [17], short-wavelength membrane fluctuations deviate from two-dimensional predictions due to finite thickness fluctuations [18], and membrane permeability to small solutes decreases systematically with increasing thickness [19]. To accurately describe the physics near the membrane surfaces at these scales, models should explicitly incorporate membrane thickness.

Building upon existing two-dimensional membrane descriptions, finite thickness effects are usually incorpo-

rated through phenomenological approaches that are inherently based on the Helfrich free energy [20–29]. Such approaches have been able to explore the relaxation dynamics of membrane-fluid systems [25, 30] and reveal signatures of the membrane thickness on the nanoscopic density fluctuations, relevant to lipid bilayer structure factor measurements [24, 29, 31, 32]. While these extensions of the Helfrich energy represent progress in modeling finite thickness effects on membrane dynamics, they do not fully account for membrane-fluid coupling consistent with three-dimensional continuum mechanics.

In this Letter, we present a finite thickness membrane model that follows from a self-consistent continuum mechanics framework and describes fluctuations of bilayers in contact with fluid reservoirs. We find that shape fluctuations on the order of 1 – 10 nm are affected by membrane thickness effects, exhibiting slower decay rates than predicted by two-dimensional theories. At these length scales, we show that in-plane surface motion caused by lipid reorientations leads to pressure inversion in the bulk and the formation of two distinct types of stagnation points near the membrane: circulatory points, which do not contribute to dissipation, and extensional points,

which give rise to viscous energy loss. This latter class is characterized by bulk fluid dissipation driven by compression and expansion of the finite-thickness membrane surfaces.

*Theory*—We consider a lipid bilayer of finite thickness  $\delta$  immersed in a quiescent, incompressible viscous fluid. The bilayer is initially flat with its mid-surface located at  $z = 0$ , as shown in Fig. 1 (a)–(i). Physically, the system experiences thermal fluctuations that perturb the membrane shape and drive flows both within the membrane and in the surrounding bulk fluids. The primary quantities of interest are the membrane deformation, the in-plane lipid motion, and the hydrodynamic stresses transmitted across the membrane surfaces.

Our objective is to model how finite membrane thickness affects the relaxation dynamics of membrane shape fluctuations. In particular, we are interested in the role of differential shear stresses between the top and bottom membrane surfaces on the coupling to the surrounding fluid—phenomena not fully resolved in strictly two-dimensional membrane models. To describe this situation, we use a continuum framework for lipid membranes—originally developed in Refs. [35–37]—which systematically incorporates thickness effects through a spectral expansion in the thickness direction, leading to the  $(2+\delta)$ -dimensional equations for lipid bilayers. As shown in Fig. 1 (a)–(ii), we represent the membrane shape using the Monge gauge,  $h(x, y, t)$  [38], valid for small deviations from flatness. Under these assumptions, the membrane momentum balances and continuity conditions take the form (see SM Sec. 5.2)

$$0 = \partial_\alpha \lambda + \mu^m \nabla_s^2 v^\alpha + \mu^b [\partial_z u^\alpha + \partial_\alpha u^z], \quad (1a)$$

$$0 = \Lambda_0 \nabla_s^2 h - \frac{1}{2} k_b \nabla_s^4 h + \mu^b \delta \partial_\alpha \left( \langle \partial_z u^\alpha + \partial_\alpha u^z \rangle \right) - [p] + 2\mu^b [\partial_z u^z], \quad (1b)$$

$$0 = \partial_x v_x + \partial_y v_y, \quad (1c)$$

where  $\alpha \in \{x, y\}$ ,  $\mathbf{v}$  and  $\mathbf{u}$  are the membrane and bulk velocities, respectively,  $\lambda$  is the in-plane membrane tension enforcing mid-surface incompressibility,  $k_b$  is the bending rigidity,  $\mu^m$  and  $\mu^b$  are the membrane and bulk viscosities,  $\Lambda_0$  is the base-state membrane tension, and  $\nabla_s \equiv \partial_x \mathbf{e}_x + \partial_y \mathbf{e}_y$  is the surface gradient operator. The operators  $[\cdot]$  and  $\langle \cdot \rangle$  denote, respectively, the jump and average of bulk quantities evaluated at the membrane surfaces. The finite thickness formulation allows for both nonzero shear stresses and velocity differences between the top and bottom membrane surface, generating modes of coupling to the bulk fluid that are inaccessible to strict two-dimensional models [6–9, 39]. Lastly, the surrounding fluid obeys the incompressible Stokes equations [40, 41], appropriate for microbiological processes where the Reynolds number is often  $\mathcal{O}(10^{-6})$  [24, 42].

To nondimensionalize the system, we introduce characteristic scales:  $L$  for length,  $U$  for velocity, and  $\tau = L/U$

for time. The dimensionless parameters that arise are the Föppl–von Kármán number  $\Gamma := \Lambda_0 L^2 / k_b$ , comparing membrane tension to bending forces; the capillary number  $\text{Ca} := \mu^b U / \Lambda_0$ , contrasting viscous forces with membrane tension; the Scriven–Love number  $\text{SL} := \mu^m U L / k_b$  [43], relating membrane viscous to bending forces; and the dimensionless membrane thickness  $\ell = \delta / L$ . In dimensionless form, the governing equations become

$$0 = \partial_\alpha \lambda + \frac{\text{SL}}{\Gamma} \nabla_s^2 v^\alpha + \text{Ca} \left( [\partial_z u^\alpha + \partial_\alpha u^z] \right), \quad (2a)$$

$$0 = \nabla_s^2 h - \frac{1}{2\Gamma} \nabla_s^4 h + \text{Ca} \left( \ell \partial_\alpha \langle \partial_z u^\alpha + \partial_\alpha u^z \rangle - [p] + 2[\partial_z u^z] \right), \quad (2b)$$

$$0 = \partial_x v_x + \partial_y v_y, \quad (2c)$$

Relevant values for the material parameters found in Eqs. (1a)–(1c) are  $k_b \sim \mathcal{O}(10^2)$  pN · nm [34, 44, 45],  $\Lambda_0 \sim \mathcal{O}(10^{-4} - 10^{-1})$  pN · nm<sup>−1</sup> [43, 44, 46], with length scales ranging from  $\mathcal{O}(10^2)$  nm for vesicles to  $\mathcal{O}(1)$   $\mu\text{m}$  for cells [33, 34, 42, 43], and velocities from  $\mathcal{O}(10^{-3})$  nm/ $\mu\text{s}$  for tube pulling [43, 47, 48] to  $\mathcal{O}(10)$  nm/ $\mu\text{s}$  for bacterial gliding [49, 50]. Taking the viscosity of water for the bulk fluids, the resulting dimensionless parameters typically satisfy  $\Gamma \sim 10^{-2} - 10^3$ ,  $\text{Ca} \sim 10^{-7} - 10^2$ , and  $\ell \sim 10^{-3} - 10^{-2}$ .

To explore the membrane dynamics, we analyze the linear response of the system to small shape fluctuations. We expand all dynamical quantities into normal modes:  $f(x, y, z, t) = \sum_{\mathbf{q}} f_{\mathbf{q}}(z) e^{i\mathbf{q} \cdot \mathbf{x} + \omega(\mathbf{q})t}$ , where  $\mathbf{q} = (q_x, q_y)$  is the dimensionless in-plane wavevector,  $\omega(\mathbf{q})$  is the dispersion relation encoding the membrane dynamical response, and surface quantities such as the displacement field  $h(x, y, t)$  are evaluated at  $z = 0$ . By applying classical no-slip boundary conditions between the membrane and the bulk fluids, while allowing for differential shear at the two membrane surfaces, and assuming decay of bulk velocities and pressures far from the membrane, we solve Eqs. (2a)–(2c) to find an expression for the dispersion relation  $\omega(\mathbf{q})$  (see SM Sec. 5.2 for details),

$$\omega(\mathbf{q}) = -\frac{\frac{1}{2}q^3 + \Gamma q}{\Gamma \text{Ca} (4 + q^2 \ell^2)}. \quad (3)$$

The form of Eq. (3) explicitly includes in the denominator membrane thickness effects, i.e.,  $q^2 \ell^2$ , on the relaxation dynamics of the membrane shape, a result that we proceed to explore in greater detail in the following section of this letter.

*Results*—To understand the implications of membrane thickness on its dynamic response, we proceed to analyze the regimes of the dispersion relation  $\omega(\mathbf{q})$ , as shown in Fig. 1 (b). We observe three distinct regions in the dispersion relation, separated by the crossover wavenumbers  $q_1 = \sqrt{2\Gamma} = 1.14$  and  $q_2 = 2/\ell = 100$  for the choice of parameters in Fig. 1. For  $q \ll q_1$ , membrane shape fluctuations are dominated by tension and relax according to

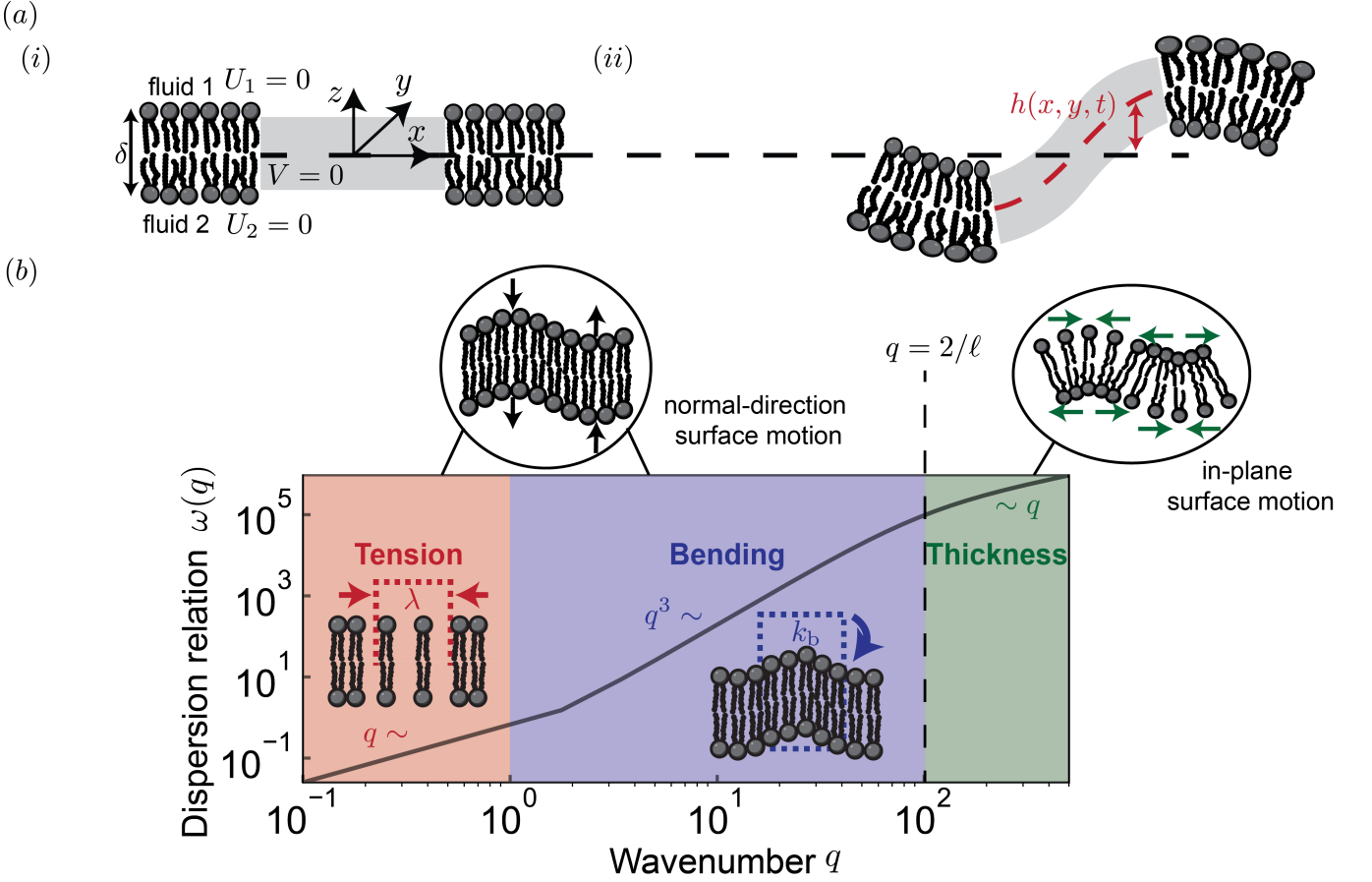


FIG. 1. (a)–(i) The base state of the linear response problem. The membrane is stationary and embedded in a quiescent fluid. (a)–(ii) The perturbed state, where the membrane mid-surface is displaced by the height field  $h(x, y, t)$ . (b) The dispersion relation for finite thickness, nearly flat membranes, as given by Eq. (3). The tension regime crosses over into bending at  $q_1 = \sqrt{2\Gamma} = 1.14$  and the viscous crossover occurs at  $q_2 = 2/\ell = 100$ , where  $\Gamma = \Lambda_0 L^2/k_b$  and  $\ell = \delta/L$ . The elastic response is characterized by a tension that maintains mid-surface incompressibility and a bending modulus that penalizes moments generated about the membrane due to curvature. In the tension and bending regimes, motion at the membrane surfaces is primarily normal to the mid-surface and corresponds to height decay, whereas in the thickness regime, in-plane motion plays a dominant role in governing dissipation, arising from density relaxation. Therefore, the viscous mechanism that dissipates membrane fluctuations transitions from normal to in-plane drag around the wavenumber  $q = \ell/2$ . This shift in dissipation mechanism is only captured by a finite thickness theory that explicitly evaluates boundary conditions at the membrane surfaces, where the strongest bulk flows at the membrane interface occur in-plane at high wavenumbers. We choose as physical parameters  $L = 200$  nm,  $k_b = 62$  pN · nm,  $\Lambda_0 = 10^{-3}$  pN · nm $^{-1}$ , and  $\delta = 4$  nm, and  $\mu^b = 10^{-3}$  pN · nm $^{-2}$  ·  $\mu$ s [33, 34].

$\omega(q) \sim q$ . For  $q_1 \ll q \ll q_2$ , bending-dominated modes govern the relaxation dynamics, decaying as  $\omega(q) \sim q^3$ . In the short wavelength regime where  $q \gg q_2$ , the mechanism for membrane relaxation shifts from viscous dissipation primarily via normal forces—such as pressure differences across the membrane—to dissipation dominated by in-plane forces arising from membrane surface shear stresses at the interfaces with the bulk, as illustrated in Fig. 1–(b). These shear stresses appear as  $\mathcal{O}(\ell)$  terms in Eq. (1b) and develop due to lipid reorientation and resultant bulk tangential flows at the membrane-fluid interfaces. This in-plane viscous dissipation is explicitly captured by finite-thickness theories but not by strict

two-dimensional theories [45, 51–53], indicating a novel mechanism by which membrane thickness slows down the response to thermally-induced fluctuations.

To understand these thickness effects on the hydrodynamic response for  $q > q_2$ , we consider  $q = 300$  and examine the induced bulk flow fields near the membrane surfaces. Figures 2 (a)–(i) & (ii) show the velocity vector fields along with their normalized magnitude for  $\ell = 0.0$  (i.e. a two-dimensional membrane) and  $\ell = 0.02$ , respectively. In Fig. 2 (a)–(i), we observe that the strictly two-dimensional membrane moves only in the normal direction. Minima in the initial perturbation push and drag bulk fluid in the positive  $z$ -direction, while max-

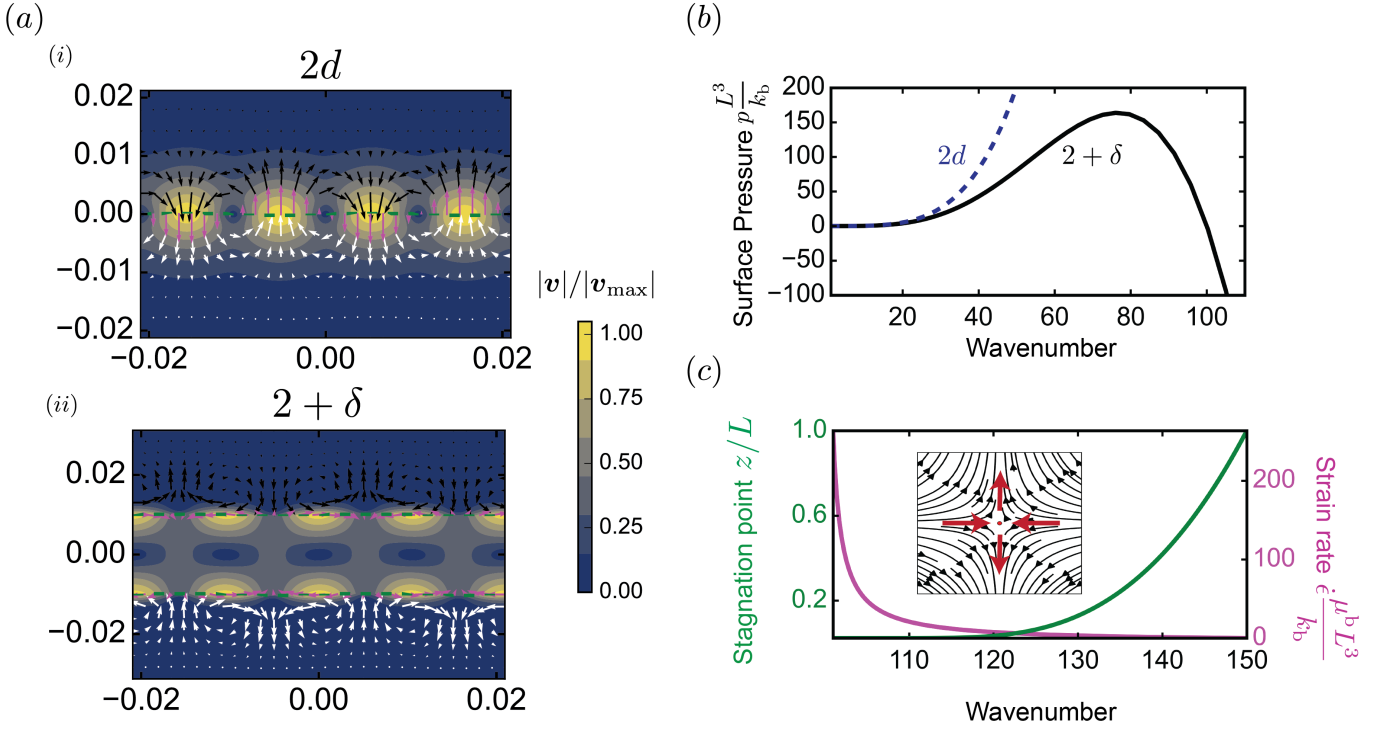


FIG. 2. (a)–(i), (ii) The instantaneous ( $t = 0$ ) flow fields induced by a mode with  $q = 300 \gg q_2$  for the two- and  $(2 + \delta)$ -dimensional theories, respectively. For clarity and the sake of comparison, we do not show the intramembrane profiles in (ii). The dominant surface motion in the two-dimensional theory is normal to the membrane and corresponds to height field relaxation while in the  $(2 + \delta)$ -dimensional theory it is tangential and corresponds to lipid reorientations. Additionally, vortices develop in the bulk when thickness is included. (b) The surface perturbed pressure at  $(x, z) = (\pi/2q, \ell/2)$  as a function of wavenumber for the 2d- and  $(2 + \delta)$ -dimensional theories. Inclusion of finite thickness modulates the pressure, which exhibits inversion at  $q = q_2 = 2/\ell$ . This signifies local flow direction reversal, which is attributed to bulk incompressibility and local in-plane flows in the thickness-dominated regime. (c) The extensional flow stagnation point position and strain rate as a function of wavenumber. We plot only for  $q > q_2$  the predicted stagnation point location is unphysical for lower wavenumbers. As the membrane surface in-plane deformations relax faster at higher wavenumbers, the stagnation points approach the membrane and their strain rate increases. The bulk circulations become increasingly localized near the membrane surface as the wavenumber increases. Including finite thickness allows us to resolve the hydrodynamics local to the membrane. The same parameters as in Fig. 1 are used here. The capillary number  $Ca$  is set to 1.

ima do so in the opposite direction, generating circular flow patterns around the membrane as a consequence of incompressibility in the bulk. While we only show flow fields for  $q = 300$ , the qualitative nature of the hydrodynamic response of the strict two-dimensional membrane is independent of the wavenumber (see SM Sec. 6.2).

Finite thickness is expected to affect the hydrodynamic response for  $q > q_2$ , as alluded to in the analysis of the dispersion relation. This is evident in Fig. 2 (a)–(ii), where we observe the emergence of in-plane motion at the membrane-fluid interfaces. This phenomenon arises due to membrane surface compression and expansion that necessarily accompany bending. While curvature effects are included in both the strict two-dimensional and the  $(2 + \delta)$ -dimensional theories, the latter improves upon the former by allowing us to resolve the three-dimensional nature of bending by incorporating finite thickness explicitly. To explore the consequences of these thickness effects, we seek to understand the hydrodynamic response

of the bulk fluid.

In the thickness-dominated regime, in-plane motion of the membrane surfaces induces in-plane fluid flow through no-slip conditions. Consequently, mass conservation in the bulk fluids necessitates the formation of circulations that appear near the top and bottom surfaces of finite thickness membranes. To further understand how membrane thickness affects the hydrodynamic response, we examine how the pressure at the membrane crests changes with increasing  $q$ , as shown in Fig. 2 (b) (see SM Sec 5.2 for details on the pressure derivation). In the case of the strict two-dimensional membrane, we find that the pressure monotonically increases as the fluctuation wavelength decreases. However, when the finite thickness nature of a membrane is considered, the pressure exhibits a maximum for  $q < q_2$  and changes sign at  $q = 2/\ell = 100$ . This pressure reversal phenomenon indicates that flow reversal occurs in the vicinity of the membrane. Because the flows change direction, we ob-

serve the appearance of two kinds of stagnation points, as shown in Fig. 2 (a)–(ii) and SM Sec. 6.3. We label the two as ‘circulatory’ and ‘extensional’ flow stagnation points based on the flow patterns observed in Fig. 2 (a)–(ii).

We characterize the nature of the two stagnation points by examining the strain rate tensor  $D_{ij} = (\partial_i u_j + \partial_j u_i)/2$ . For circulatory stagnation points, the local strain rate vanishes, indicating that these points do not contribute to the viscous dissipation responsible for dynamic slowing in the thickness-dominated regime (see Sec. 6.3 SM). However, at the other stagnation points, the strain rate tensor has non-zero diagonal components  $D_{11} = -D_{22} = \dot{\epsilon}$ , indicating that the flows at these points are extensional in nature. We find that the extensional points are located at

$$(x, z)_{\text{ext}}^{\pm} = \left( (2n+1)\frac{\pi}{2q}, \pm \frac{\ell}{2} \pm \frac{2}{q(\ell q - 2)} \right), \quad n \in \mathbb{Z}, \quad (4)$$

and their strain rate is given by

$$\dot{\epsilon} = \frac{1}{2} \omega h_0 (\ell q - 2) \exp\left(\frac{-2}{\ell q - 2}\right). \quad (5)$$

Figure 2 (c) shows  $\dot{\epsilon}$  and  $z_{\text{ext}}^+$  for  $n = 0$  in terms of the wavenumber  $q$ . When  $q \sim q_2$ , the stagnation points appear with negligible strain rate infinitely far away from the membrane surface. With increasing  $q$ , the stagnation points become localized near the membrane surfaces, and exhibit increasingly large extensional strain rates. In this large wavenumber regime, in-plane deformation gradients at the membrane surfaces couple to the bulk fluid and give rise to the observed stagnation point phenomena.

*Discussion*—Previously, we showed that explicitly accounting for the membrane thickness modifies the coupling between the membrane and surrounding bulk fluids, resulting in modified dynamics of bending mode relaxation (Fig. 1 (b)). As a result, fluctuations with  $q > q_2 = 2/\ell$  exhibit pressure inversion at the membrane surfaces (Fig. 2 (b)), which is marked by the development of vortices and local stagnation points associated with circulatory and extensional flows (Fig. 2 (c)). In particular, the extensional flow points display a mode of bulk fluid viscous dissipation caused by the compression and extension of the finite-thickness membrane during bending (Fig. 1 (c)–(ii)). This mode contributes to a decrease in the ability of the bulk fluid to dissipate membrane fluctuations, and thus leads to the dynamic slowing down of bending modes in the “thickness” regime.

Previous works on modeling lipid bilayers have employed modified Helfrich approaches to incorporate thickness effects into membrane dynamics [20, 21, 24, 25, 28, 30, 54]. The most common approach is the inter-monolayer slip (IS) model [20, 21, 23], which assumes coupled motion of independent bilayer leaflets and introduces a phenomenological friction coefficient to account for inter-leaflet dissipation as the monolayers slide

past one another. While both the IS model and the  $(2 + \delta)$ –dimensional theory predict in-plane flows at the membrane surfaces [25], the underlying mechanisms are distinct. The IS model attributes these flows to density relaxation and monolayer slip (see Figs. 9 (a)–(c) in SM Sec. 7), whereas the present work predicts them to be a consequence of lipid reorientations and three-dimensional hydrodynamic coupling, as shown in Fig. 1 (c)–(ii). A detailed comparison between these approaches, including their respective dispersion relations and induced flow fields, is provided in Sec. 7 of the SM.

Experimentally, membrane dynamics on nanometer length scales are often probed through density fluctuations via structure factor measurements [24, 29, 55–58]. Such analyses require a statistical description of membrane relaxation across a wide range of length scales, including those at the membrane thickness. The dispersion relation  $\omega(q)$  of Eq. (3) provides the connection between the current work and the statistics of membrane fluctuations, which are measured experimentally via techniques such as neutron spin echo, dynamic light scattering, or flicker spectroscopy [29, 44, 53, 59]. To link  $\omega(q)$  with the dynamics of fluctuating membranes, we express it as a ratio between conservative and dissipative parts as

$$\omega(q) = -\frac{\kappa_q^{\text{eff}}}{\zeta_q^{\text{eff}}} = -\frac{(\frac{1}{2}q^4 + \Gamma q^2)}{\text{Ca}\Gamma q(4 + q^2\ell^2)}, \quad (6)$$

where  $\kappa_q^{\text{eff}} \equiv \frac{1}{2}q^4 + \Gamma q^2$  represents the elastic response of the membrane due to out-of-plane bending, and  $\zeta_q^{\text{eff}} \equiv \text{Ca}\Gamma q(4 + q^2\ell^2)$  encodes all dissipative processes associated with coupling to the bulk fluid. This form motivates us to model the evolution of height fluctuations  $h_q$  through an effective overdamped Langevin equation as

$$0 = -\zeta_q^{\text{eff}} \partial_t h_q(t) - \kappa_q^{\text{eff}} h_q(t) + f_q(t), \quad (7)$$

where  $f_q(t)$  is a Gaussian distributed random force with  $\langle f_q(t) \rangle = 0$  and  $\langle f_q(t) f_{-q}(t') \rangle = 2k_B T \zeta_q^{\text{eff}} \delta(t - t')$  [60]. Reinterpreting our results in the context of statistical mechanics, we can treat  $\kappa_q^{\text{eff}}$  as an effective spring constant governing membrane fluctuations and  $\zeta_q^{\text{eff}}$  as an effective friction due to bulk coupling. Through the lens of the fluctuation-dissipation theorem [60–62], the balance between these two terms dictates how thermal fluctuations relax. At high wavenumbers ( $q > q_2$ ), bulk shear forces at the membrane surfaces introduce an additional dissipation mechanism that modifies  $\zeta_q^{\text{eff}}$ , leading to altered relaxation dynamics. This suggests that measurable fluctuation spectra may deviate from predictions based on strictly two-dimensional membrane models, particularly at nanometer length scales. Based on these insights, we expect measurements for vesicles with radius  $L = 200$  nm, which leads to  $\text{Ca} = 1$  and  $\Gamma = 0.65$ , to exhibit thickness effects on the relaxation dynamics for scattering with  $\lambda_{\text{scatter}} \lesssim 2\pi L/q_2 \approx 12$  nm. The timescale associ-

ated with this length scale is  $\tau = \mu^b \lambda_{\text{scatter}}^3 / \Gamma k_b \approx 40$  ns for the values used in Fig. 1.

Regarding the relevance of our findings, we expect that they have implications for biological processes such as mechanosensitive protein function and intercellular contact. For instance, it has recently been observed that increased membrane thickness correlates with reduced permeability to solute molecules [19]. While multiple factors likely contribute to this effect, our results suggest that nanoscale circulations induced by finite thickness effects could potentially influence local mixing near the membrane. Such flows may, in turn, affect solute concentration gradients, which could play a role in permeability regulation. A more detailed investigation would be required to determine the extent to which hydrodynamics contribute to mass transport across lipid bilayer membranes. Additionally, the predicted pressure inversion phenomenon at nanoscales, Fig. 2-(b), can lead to hydrodynamic-related forces [63] that might mediate intercellular contact and affect intermembrane junction fluctuations [64, 65]. Further experimental studies on free-standing and confined membranes are necessary in revealing the relevance of finite thickness effects on the discussed processes.

*Conclusion*—In summary, we have shown that the finite thickness of lipid bilayers affects how they couple with the surrounding media. In particular, shear forces caused by lipid reorientations during bending develop at the membrane surfaces, resulting in in-plane flows that are not observed in direct two-dimensional membrane models. This mechanism leads to a redistribution of momentum between the membrane and bulk fluid, where in-plane lipid motion generates shear stresses that induce circulatory and extensional flow patterns in the surrounding fluid. For fluctuations on the order of the membrane thickness, we show that this coupling results in pressure inversion at the membrane surfaces, indicating the existence of flow reversal in the vicinity of the bilayer. Stagnation points associated with bulk fluid circulatory and extensional flows mark where the flow reversal occurs. Finally, we have shown that our dispersion relation provides a direct link between continuum membrane mechanics and measurable fluctuation spectra, which can be probed using neutron spin echo or dynamic light scattering.

*Acknowledgments* ZGL and YADO would like to acknowledge discussions with Kranthi K. Mandadapu. ZGL and YADO were financially supported by the University of California, Berkeley and the Director, Office of Science, Office of Basic Energy Sciences, of the U.S. Department of Energy under contract No. DEAC02-05CH11231. ZGL was supported partially by the National Science Foundation through NSF-DFG 2223407 and the Deutsche Forschungsgemeinschaft (German Research Foundation)—509322222. DF (dfrag) acknowledges Princeton University and the Department of Chem-

ical and Biological Engineering for financial support provided through their start-up funding.

---

\* zl4808@princeton.edu

† yadomar@mit.edu

‡ dimfraged@gmail.com & dfrag@princeton.edu

- [1] K. Iwasa and I. Tasaki, *Biochemical And Biophysical Research Communications* **95**, 1328 (1980).
- [2] S. Watanabe, B. R. Rost, M. Camacho-Pérez, M. W. Davis, B. Söhl-Kielczynski, C. Rosenmund, and E. M. Jorgensen, *Nature* **504**, 242 (2013).
- [3] Z. Shi and T. Baumgart, *Nature Communications* **6**, 5974 (2015).
- [4] A. Carlson and L. Mahadevan, *Physics Of Fluids* **27** (2015).
- [5] T. Ling, K. C. Boyle, V. Zuckerman, T. Flores, C. Ramakrishnan, K. Deisseroth, and D. Palanker, *Proceedings Of The National Academy Of Sciences* **117**, 10278 (2020).
- [6] W. Helfrich, *Zeitschrift Fur Naturforschung - Section C Journal Of Biosciences* **28**, 693 (1973).
- [7] D. Steigmann, *Archive For Rational Mechanics And Analysis* **150**, 127 (1999).
- [8] M. Deserno, *Chemistry And Physics Of Lipids* **185**, 11 (2015), publisher: Elsevier Ireland Ltd.
- [9] A. Sahu, R. A. Sauer, and K. K. Mandadapu, *Physical Review E* **96**, 1 (2017).
- [10] J. Liu, M. Kaksonen, D. G. Drubin, and G. Oster, *Proceedings Of The National Academy Of Sciences* **103**, 10277 (2006).
- [11] A. Agrawal and D. J. Steigmann, *Biomechanics And Modeling In Mechanobiology* **8**, 371 (2009).
- [12] S. Dmitrieff and F. Nédélec, *PLOS Computational Biology* **11**, e1004538 (2015).
- [13] Y. A. Omar, A. Sahu, R. A. Sauer, and K. K. Mandadapu, *Biophysical Journal* **119**, 1065 (2020).
- [14] P. Saffman and M. Delbrück, *Proceedings Of The National Academy Of Sciences* **72**, 3111 (1975).
- [15] A. Agrawal and D. J. Steigmann, *Zeitschrift Für Angewandte Mathematik Und Physik* **62**, 549 (2011).
- [16] R. Samanta and N. Oppenheimer, *Physics of Fluids* **33**, 051906 (2021), <https://pubs.aip.org/aip/pof/article-pdf/doi/10.1063/5.0052213/19762549/051906-1.online.pdf>.
- [17] R. Phillips, T. Ursell, P. Wiggins, and P. Sens, *Nature* **459**, 379 (2009).
- [18] A. C. Woodka, P. D. Butler, L. Porcar, B. Farago, and M. Nagao, *Physical Review Letters* **109**, 058102 (2012).
- [19] J. Frallicciardi, J. Melcr, P. Siginou, S. J. Marrink, and B. Poolman, *Nature Communications* **13**, 1605 (2022).
- [20] U. Seifert and S. A. Langer, *Europhysics Letters* **23**, 71 (1993).
- [21] E. Evans and A. Yeung, *Chemistry And Physics Of Lipids* **73**, 39 (1994).
- [22] R. Merkel, E. Sackmann, and E. Evans, *Journal De Physique* **50**, 1535 (1989).
- [23] A. Yeung and E. Evans, *Journal De Physique Ii* **5**, 1501 (1995).
- [24] M. C. Watson, Y. Peng, Y. Zheng, and F. L. Brown, *The Journal Of Chemical Physics* **135** (2011).

- [25] J.-b. Fournier, International Journal Of Non-Linear Mechanics **75**, 67 (2015).
- [26] M. M. Terzi and M. Deserno, The Journal Of Chemical Physics **147** (2017).
- [27] K. V. Pinigin, P. I. Kuzmin, S. A. Akimov, and T. R. Galimzyanov, Physical Review E **102**, 042406 (2020).
- [28] L. Deseri, M. D. Piccioni, and G. Zurlo, Continuum Mechanics And Thermodynamics **20**, 255 (2008).
- [29] H. A. Faizi, R. Granek, and P. M. Vlahovska, Proceedings of the National Academy of Sciences **121**, e2413557121 (2024), <https://www.pnas.org/doi/pdf/10.1073/pnas.2413557121>.
- [30] M. Rahimi and M. Arroyo, Physical Review E **86**, 011932 (2012).
- [31] E. G. Kelley, M. P. Frewein, O. Czakkell, and M. Nagao, Symmetry **15**, 191 (2023).
- [32] M. Nagao, E. G. Kelley, R. Ashkar, R. Bradbury, and P. D. Butler, The Journal Of Physical Chemistry Letters **8**, 4679 (2017).
- [33] B. Alberts, J. Watson, J. Lewis, M. Raff, K. Roberts, A. Johnson, and P. Walter, *Molecular Biology of the Cell* (Garland Science, New York City, 2002).
- [34] R. Phillips, Physics Of Biological Membranes , 73 (2018).
- [35] Y. A. Omar, Z. G. Lipel, and K. K. Mandadapu, Physical Review E **109**, 054401 (2024).
- [36] Y. A. Omar, Z. G. Lipel, and K. K. Mandadapu, Arxiv Preprint Arxiv:2309.03863 (2023).
- [37] Y. A. Omar, Z. G. Lipel, and K. K. Mandadapu, Arxiv Preprint Arxiv:2501.11612 (2025).
- [38] G. Monge, *Application de l'analyse à la géométrie* (Bernard, Paris, 1807).
- [39] P. B. Canham, Journal Of Theoretical Biology **26**, 61 (1970).
- [40] J. Happel and H. Brenner, Low Reynolds Number Hydrodynamics. With Special Applications To Particulate Media. M. Nijhoff, Leiden (1983).
- [41] S. Kim and S. J. Karrila, *Microhydrodynamics: principles and selected applications*, Butterworth-Heinemann series in chemical engineering (Butterworth-Heinemann, Boston, 1991).
- [42] E. M. Purcell, American Journal Of Physics **45**, 3 (1977).
- [43] A. Sahu, A. Glisman, J. Tchoufag, and K. K. Mandadapu, Physical Review E **101**, 052401 (2020).
- [44] J. Pécréaux, H.-g. Döbereiner, J. Prost, J.-f. Joanny, and P. Bassereau, The European Physical Journal E **13**, 277 (2004).
- [45] S. C. Takatori and A. Sahu, Physical Review Letters **124**, 158102 (2020).
- [46] J. Dai, M. P. Sheetz, X. Wan, and C. E. Morris, Journal Of Neuroscience **18**, 6681 (1998).
- [47] Z. Shi, Z. T. Graber, T. Baumgart, H. A. Stone, and A. E. Cohen, Cell **175**, 1769 (2018).
- [48] C. Leduc, O. Campàs, K. B. Zeldovich, A. Roux, P. Jolimaitre, L. Bourel-Bonnet, B. Goud, J.-f. Joanny, P. Bassereau, and J. Prost, Proceedings Of The National Academy Of Sciences **101**, 17096 (2004).
- [49] B. Nan and D. R. Zusman, Annual Review Of Genetics **45**, 21 (2011).
- [50] J. Tchoufag, P. Ghosh, C. B. Pogue, B. Nan, and K. K. Mandadapu, Proceedings Of The National Academy Of Sciences **116**, 25087 (2019).
- [51] W. Helfrich and R. m. Servuss, Il Nuovo Cimento D **3**, 137 (1984).
- [52] M. Mutz and W. Helfrich, Journal De Physique **51**, 991 (1990).
- [53] F. Brochard and J. Lennon, Journal De Physique **36**, 1035 (1975).
- [54] T. R. Galimzyanov, P. V. Bashkirov, P. S. Blank, J. Zimmerberg, O. V. Batishchev, and S. A. Akimov, Soft Matter **16**, 1179 (2020).
- [55] A. G. Zilman and R. Granek, Chemical Physics **284**, 195 (2002).
- [56] Z. Yi, M. Nagao, and D. P. Bossev, Journal Of Physics: Condensed Matter **21**, 155104 (2009).
- [57] M. Nagao, Physical Review E **80**, 031606 (2009).
- [58] E. G. Kelley, M. P. Frewein, O. Czakkell, and M. Nagao, Symmetry **15**, 191 (2023).
- [59] C. Monzel and K. Sengupta, Journal Of Physics D: Applied Physics **49**, 243002 (2016).
- [60] R. Granek, Journal De Physique **7**, 1761 (1997).
- [61] R. Kubo, Reports On Progress In Physics **29**, 255 (1966).
- [62] D. Lacoste and A. W. C. Lau, Europhysics Letters **70**, 418 (2005).
- [63] D. Bartolo, A. Ajdari, J.-B. Fournier, and R. Golestanian, Physical Review Letters **89**, 230601 (2002).
- [64] K. Liu, B. Chu, J. Newby, E. L. Read, J. Lowengrub, and J. Allard, PLOS Computational Biology **15**, e1006352 (2019).
- [65] L. C.-l. Lin, J. T. Groves, and F. L. Brown, Biophysical Journal **91**, 3600 (2006).